



Contents lists available at SciVerse ScienceDirect

## Physics of the Earth and Planetary Interiors

journal homepage: [www.elsevier.com/locate/pepi](http://www.elsevier.com/locate/pepi)Metastable high-pressure transformations of orthoferrosilite  $\text{Fs}_{82}$ Przemyslaw Dera<sup>a,e,\*</sup>, Gregory J. Finkelstein<sup>b</sup>, Thomas S. Duffy<sup>b</sup>, Robert T. Downs<sup>c</sup>, Yue Meng<sup>d</sup>, Vitali Prakapenka<sup>a</sup>, Sergey Tkachev<sup>a</sup><sup>a</sup> Center for Advanced Radiation Sources, University of Chicago, Argonne National Laboratory, 9700 S. Cass Ave., Bldg. 434, Argonne, IL 60439, USA<sup>b</sup> Department of Geosciences, Princeton University, USA<sup>c</sup> Geology Department, University of Arizona, USA<sup>d</sup> High Pressure Collaborative Access Team, Carnegie Institution of Washington, USA<sup>e</sup> Hawaii Institute of Geophysics and Planetology, School of Ocean and Earth Science and Technology, University of Hawaii at Manoa, USA

## ARTICLE INFO

## Article history:

Received 3 February 2013

Received in revised form 11 June 2013

Accepted 13 June 2013

Available online xxx

## Keywords:

Ferrosilite

Enstatite

Pyroxenes

High-pressure phase transition

Upper mantle

Synchrotron single-crystal X-ray diffraction

## ABSTRACT

High-pressure single-crystal X-ray diffraction experiments with natural ferrosilite  $\text{Fs}_{82}$  ( $\text{Fe}^{2+}_{0.82}\text{Mg}_{0.16}\text{Al}_{0.01}\text{Ca}_{0.01}(\text{Si}_{0.99}\text{Al}_{0.01})\text{O}_3$  orthopyroxene (opx) reveal that at ambient temperature the sample does not transform to the clinopyroxene (cpx) structure, as reported earlier for a synthetic  $\text{Fs}_{100}$  end-member (Hugh-Jones et al., 1996), but instead undergoes a series of two polymorphic transitions, first above 10.1(1) GPa, to the monoclinic  $\text{P}2_1/c$  phase  $\beta$ -opx (distinctly different from both  $\text{P}2_1/c$  and  $\text{C}2/c$  cpx), also observed in natural enstatite (Zhang et al., 2012), and then, above 12.3(1) GPa to a high-pressure orthorhombic  $\text{Pbca}$  phase  $\gamma$ -opx, predicted for  $\text{MgSiO}_3$  by atomistic simulations (Jahn, 2008). The structures of phases  $\alpha$ ,  $\beta$  and  $\gamma$  have been determined from the single-crystal data at pressures of 2.3(1), 11.1(1), and 14.6(1) GPa, respectively. The two new high-pressure transitions, very similar in their character to the  $\text{P}2_1/c$ – $\text{C}2/c$  transformation of cpx, make opx approximately as dense as cpx above 12.3(1) GPa and significantly change the elastic anisotropy of the crystal, with the [100] direction becoming almost twice as stiff as in the ambient  $\alpha$ -opx phase. Both transformations involve mainly tetrahedral rotation, are reversible and are not expected to leave microstructural evidence that could be used as a geobarometric proxy. The high  $\text{Fe}^{2+}$  content in  $\text{Fs}_{82}$  shifts the  $\alpha$ – $\beta$  transition to slightly lower pressure, compared to  $\text{MgSiO}_3$ , and has a very dramatic effect on reducing the (meta) stability range of the  $\beta$ -phase.

© 2013 Elsevier B.V. All rights reserved.

## 1. Introduction

Pyroxenes are among the most important minerals of the Earth's upper mantle and account for approximately 20% of the composition of this layer by volume (Frost, 2008). The pyroxene structure is composed of close-packed layers of O atoms with alternating tetrahedral and octahedral layers that accommodate a variety of different cations ranging from the typical divalent  $\text{Mg}^{2+}$ ,  $\text{Fe}^{2+}$ ,  $\text{Ca}^{2+}$ ,  $\text{Mn}^{2+}$ , through monovalent  $\text{Na}^+$ , to trivalent  $\text{Al}^{3+}$ ,  $\text{Fe}^{3+}$  and  $\text{Cr}^{3+}$  without inducing major rearrangements to the topology and connectivity within the crystal. The structural and compositional flexibility is a consequence of the ability of the infinite corner-linked tetrahedral chains extending along the [001] direction to stretch or compress by rotation of the individual tetrahedra without affecting the tetrahedral bond lengths, following the rigid unit mode model (Dove et al., 1995). Because of the tetrahedral layer

flexibility cations with very different ionic radii coordinated by 4 to 8 oxygen atoms can be accommodated in the M2 sites of the octahedral layers.

Four distinct ambient polymorphs of pyroxene are known, differing in crystal symmetry and layer stacking topology, including  $\text{C}2/c$  diopside-type,  $\text{P}2_1/c$  clinoenstatite-type (lp-cpx),  $\text{Pbca}$  orthoenstatite-type ( $\alpha$ -opx), and  $\text{Pbnm}$  protoenstatite. Their structures, while easily distinguishable, are very closely related. For some compositions, e.g. in  $\text{C}2/c$  spodumene,  $\text{P}2$  and  $\text{P}2/n$  omphacites and  $\text{P}2_1ca$  lunar orthopyroxene, small symmetry distortions are found, but their topological relations to the four basic ambient structural types are easily recognizable. Because of the distinct layer stacking patterns, transitions between the principal pyroxene polymorph types are in general reconstructive and involve significant activation barriers, which lead to metastability (Downs, 2003; Thompson and Downs, 2003).

The main geologically-relevant subset of pyroxene composition space is the  $\text{MgCaSi}_2\text{O}_6$  (diopside)– $\text{MgSiO}_3$  (enstatite)– $\text{FeSiO}_3$  (ferrosilite)– $\text{CaFeSi}_2\text{O}_6$  (hedenbergite) quadrilateral. Significant (above 10%)  $\text{Ca}^{2+}$  content strongly favors the monoclinic diopside-type cpx arrangement, while at low  $\text{Ca}^{2+}$ -contents the preference between the cpx and opx structures is controlled by the pressure and

\* Corresponding author. Address: Hawaii Institute of Geophysics and Planetology, School of Ocean and Earth Science and Technology, University of Hawaii at Manoa, 1680 East West Road, POST Bldg, Office 819 EHonolulu, Hawaii 96822, USA. Tel.: +1 808 956 6347.

E-mail address: [dera@cars.uchicago.edu](mailto:dera@cars.uchicago.edu) (P. Dera).

temperature of crystallization (Lindsley, 1983). The compositions richest in  $\text{Ca}^{2+}$  do not crystallize in the pyroxene structure, but instead assume a  $\text{CaSiO}_3$  wollastonite structure.

It is widely accepted that the stable high P–T phase diagram along the enstatite-ferrosilite join is composed only of the four principal pyroxene polymorphs. However, a number of recent experimental results and theoretical predictions indicate that the orthorhombic phases if compressed at ambient temperature, rather than transforming to cpx tend to undergo a different kind of structural transformations. Raman spectroscopic experiments indicate one such transition in  $\text{En}_{100}$  at a pressure of about 10 GPa (Lin, 2003, 2004; Lin et al., 2005). A similar discontinuity in the behavior of hyperfine parameters was noted in a synchrotron Mössbauer study (Zhang et al., 2011). First principles molecular dynamics simulations of the phase behavior of  $\text{En}_{100}$  starting from the opx structure, conducted at a simulation temperature of 1000 K also revealed a lack of transformation to the monoclinic cpx form, resulting from the large activation barrier for this reconstructive transition. Instead, two possible new metastable displacive polymorphic transitions to HP-OEn2 with space group  $P2_1ca$  at 9 GPa and further, to HP-OEn1 with space group  $Pbca$  (different than the ambient structure) at 20 GPa were predicted (Jahn, 2008).<sup>1</sup> The two metastable transformations involve gradual rotation of the tetrahedra in the O-type tetrahedral chains, characteristic of the low pressure OEn phase to the S-type. Finally, a recent single crystal study using natural samples with  $\text{OEn}_{87}$  composition revealed that the phase above 10 GPa is monoclinic (space group  $P2_1/c$ ), but preserves the opx structure topology, with the main structural change being conversion of 25% of the Si-chains from the O to S configuration (Zhang et al., 2012).

The two main processes limiting the geophysical occurrence of pyroxenes in the Earth lower mantle at depths below the transition zone are believed to be dissolution of pyroxene into the garnet structure and the decomposition reaction to free  $\text{SiO}_2$  and high-pressure phases of  $(\text{Mg, Fe})_2\text{SiO}_4$  (Akimoto and Syono, 1970; Ming and Bassett, 1975; Liu, 1976). The boundary of the decomposition reaction coincides with the coesite-stishovite transition of  $\text{SiO}_2$ , which increases the density of the  $\text{SiO}_2$  decomposition product phase by about 30%. At about the same pressure where coesite transforms to stishovite the spinel-type Fe-ringwoodite becomes the stable form of  $\text{Fe}_2\text{SiO}_4$ , however, the volume change associated with this transition ( $\sim 8\%$ ) is smaller than in  $\text{SiO}_2$ . The decomposition reaction is characterized by a significant activation barrier, and temperatures above 1000 K are needed to initiate the process. The temperature required for decomposition also increases with pressure.

Pyroxenes are abundant in the oceanic crust, which is subducted into the upper mantle at convergent margins (Poli and Schmidt, 2002). While the displacive polymorphic transformations of opx are most likely only between metastable phases, they may have some relevance for deep Earth environments that significantly depart from the standard continental geotherm, such as cold subducted slabs. Some geophysical models (e.g. Bina et al., 2001) assume that subduction can extend to depths greater than 800 km (corresponding to pressures above 30 GPa), with the coldest part of the slab remaining below 1000 K. Orthopyroxene, once stably formed in the oceanic crust, could be metastably transported within the subducting slab to these very significant depths, and experience pressures higher than 10 GPa while still at temperatures lower than the metastable boundaries of polymorphic

conversion, dissolution or decomposition (e.g. Nishi et al., 2008 recently demonstrated significant kinetic inhibition of the pyroxene dissolution in garnet at cold subducted slab conditions, at depths exceeding 500 km). As a consequence, understanding of the nature and properties of the high-pressure opx polymorphs may be important in modeling the geophysical behavior of subduction zones (e.g. Bina et al., 2001; Akashi et al., 2009).

$\text{FeSiO}_3$  ferrosilite (Fs) is an end-member of the principal pyroxene quadrilateral, and as such is very important in understanding the general crystal chemical and phase stability trends. Pure  $\text{FeSiO}_3$  has not been reported to occur in nature, but minerals with high Fe/Mg ratios are not uncommon in high-pressure rocks (Bown, 1965; Jaffe et al., 1978; Schreyer et al., 1978; Brothers and Yokoyama, 1990; Young and Cuthbertson, 1994).

Thus far only three polymorphs of synthetic  $\text{Fs}_{100}$  have been observed at ambient conditions, including opx, lp-cpx and Fs-III (Lindsley et al., 1964). Subsequent structural investigation of these polymorphs revealed that Fs-III (space group P-1) has a pyroxenoid structure (Weber, 1983). High temperature Brillouin scattering study with natural low-Fe OEn at ambient pressure revealed existence of a possible reversible displacive transition to yet unknown high temperature phase at  $\sim 1100^\circ\text{C}$  (Jackson et al., 2004). Unlike OEn, pure OFs was found to convert to cpx at about 4.2 GPa at ambient temperature through a reconstructive transition (Hugh-Jones et al., 1996). An OFs sample with intermediate composition,  $\text{Fs}_{45}\text{En}_{46}\text{Ts}_9$  (Ts indicates Tschermak substitution), on the other hand, did not undergo the opx-cpx conversion at ambient temperature up to 9.5 GPa (Nestola et al., 2008). To understand the effect of high  $\text{Fe}^{2+}$  content on the opx-cpx and  $\alpha$ - $\beta$ -opx transitions we conducted diamond anvil cell single-crystal synchrotron X-ray diffraction experiments with a natural  $\text{OFs}_{82}$  sample to 32 GPa.

## 2. Experimental methods

The natural  $\text{Fs}_{82}$  sample used in our study is from the University of Arizona RRUFF project collections (RRUFF.info/R070386) from a locality in Greenland. This sample was previously used in the thermodynamic study of Mg–Fe order–disorder in orthopyroxenes by Saxena and Ghose (1971), and was referred to as sample XYZ in the Ramberg and DeVore (1951) study of Fe–Mg distribution between olivines and pyroxenes. Electron microprobe analysis (EMPA) indicated a composition  $(\text{Fe}^{2+}_{0.82}\text{Mg}_{0.16}\text{Al}_{0.01}\text{Ca}_{0.01})\text{-(Si}_{0.99}\text{Al}_{0.01}\text{O}_3$ . Unit cell parameters determined on a single crystal fragment of the sample using a Bruker D8 diffractometer at the University of Arizona were  $a = 18.383(1)\text{ \AA}$ ,  $b = 9.012(1)\text{ \AA}$ ,  $c = 5.2344(6)\text{ \AA}$ , with a volume of  $867.2(3)\text{ \AA}^3$ . This volume is approximately 1% smaller than for pure synthetic  $\text{OFs}_{100}$  end member (Bass and Weidner, 1984). The bulk composition of the sample was close to the sample S95 of Nestola et al. (2008),  $(\text{Fe}^{2+}_{0.91}\text{Mg}_{0.93}\text{Ca}_{0.01}\text{Mn}_{0.02}\text{Al}_{0.08}\text{Fe}^{3+}_{0.07})(\text{Si}_{0.85}\text{Al}_{0.15}\text{O}_3$ , with  $a = 18.2920(3)\text{ \AA}$ ,  $b = 8.8637(4)\text{ \AA}$ ,  $c = 5.2179(3)\text{ \AA}$ , and  $V = 845.99(6)\text{ \AA}^3$ , however, our sample had much higher  $\text{Fe}^{2+}/\text{Mg}^{2+}$  ratio, almost no ferric iron, much lower Al content (the S95 sample contained 15 mol% of trivalent cations incorporated via Tschermak substitution), and a more uniform distribution of Fe between the M1 and M2 octahedral sites, as determined by single crystal structure refinement.

Three separate in situ single-crystal X-ray diffraction experiments were carried out at experimental stations 16IDB (experiments 1 and 2) and 13IDD (experiment 3) of the Advanced Photon Source (APS), Argonne National Laboratory. In each experiment, two crystals with different orientations were loaded into the diamond anvil cell, as shown in Supplementary Fig. 1. The same 4-pin type diamond anvil cell was used in all three experiments. Diamond anvils with culets of 0.3 mm were mounted on asymmetric backing plates (cubic boron nitride towards the X-ray source

<sup>1</sup> Jahn (2008), and later Zhang et al. (2012) named the new phases of orthoenstatite HP-OEn1, HP-OEn2 and HPCN2, however, we prefer to adopt a naming convention in which the high-pressure polymorphs of opx will be referred to as  $\alpha$ -opx (ambient),  $\beta$ -opx  $\gamma$ -opx etc., to emphasize the topological relationship, which seems more important than the crystal symmetry.

and Boehler/Almax with 70 deg. total opening towards the detector). A rhenium metal gasket, preindented to a thickness of approximately 0.040 mm, was used for sample containment. The DAC was loaded with a neon pressure medium using the GSECARS/COMPRES gas loading system (Rivers et al., 2008). Pressure was estimated based on a ruby fluorescence spectrum collected at each pressure point (Mao et al., 1986). A monochromatic beam with an incident energy of 35 keV (experiments 1 and 2) or 37 keV (experiment 3), focused with a pair of Kirkpatrick-Baez mirrors to a spot of 0.003 by 0.005 mm, was used. Diffraction images were collected using a MAR165 charge coupled device (CCD) detector, placed at a sample-to detector distance of approximately 200 mm. The data collection procedure is described in Dera et al. (2011) (rotation range was  $\pm 35^\circ$ , with step size of  $1^\circ$  and exposure time of 0.5°/s). Diffraction images were analyzed using the GSE\_ADA/RVS software package (Dera et al., 2013). Because of the high incident energy and negligible sample thickness the sample absorption was ignored. Unit cell parameters measured in all three experiments are listed in Table 1.

Refined unit cell parameters from single-crystal diffraction measurements were used for equation of state (EOS) fit. For  $\alpha$ -opx and  $\gamma$ -opx the 3rd order Birch Murnaghan equation was used (Angel, 2000), with  $V_0$  of the  $\alpha$ -phase fixed to the experimentally determined value. Statistical weights equal to  $1/\sigma(V)$  were used in the fitting process. The results of EOS fitting for the two phases of opx are shown in Fig. 1, and are compared with other experimental and theoretical results for samples with compositions close to the En-Fs join in Supplementary Table 1. For the  $\beta$ -opx phase the two available pressure points were insufficient for estimation of the bulk moduli. To estimate the elastic anisotropy of the different phases of opx, a quadratic function was fit to the pressure dependence of each of the normalized unit cell parameters. The results of this fitting are shown in Fig. 1.

The structures of phases  $\alpha$ -opx,  $\beta$ -opx and  $\gamma$ -opx were refined starting from atomic coordinates of the ambient  $\alpha$ -opx Fs (Sueno et al., 1976) using the conventional least-squares crystal structure refinement approach implemented in the SHELXL program (Sheldrick, 2008). Structure refinements for the orthorhombic phases were completed with anisotropic displacement parameters for all non-oxygen atoms, whereas isotropic displacement parameters were used for all atoms in the monoclinic phase. Details of the crystal structure refinement, refined fractional coordinates for all the atoms in phases  $\alpha$ -opx,  $\beta$ -opx and  $\gamma$ -opx, bond lengths, anisotropic atomic displacement parameters and polyhedral geometry parameters are given in Supplementary Tables 2–8.

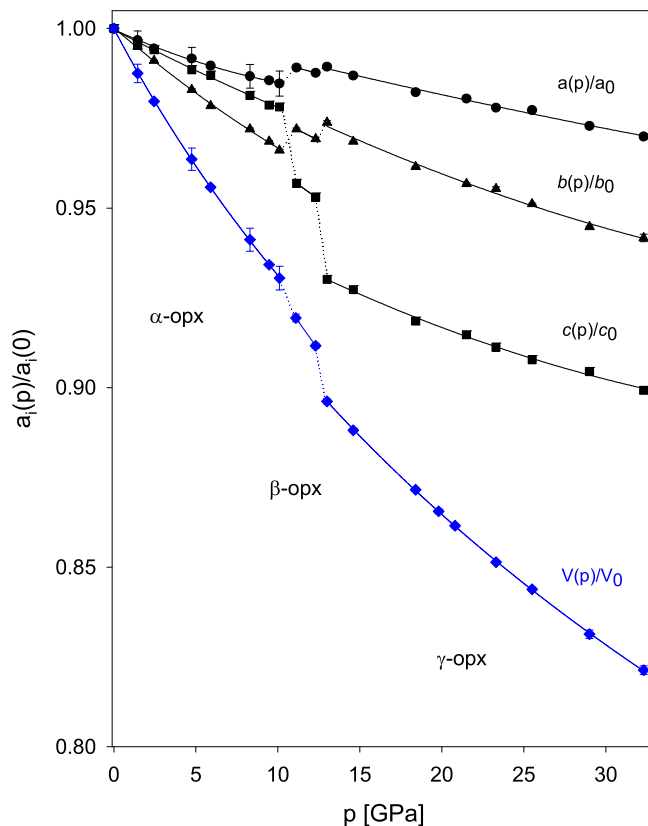


Fig. 1. Pressure evolution of normalized unit cell parameters of  $\text{Fs}_{82}$ .

The structure refinements took into account the  $\text{Fe}^{2+}/\text{Mg}^{2+}$  substitution, and refined site occupancy factors (SOF) are listed in Supplementary Table 3. For all three phases the site occupancies for the same type of site are consistent to within a few percent, suggesting that no re-distribution of cations occurs, as expected, during compression at ambient temperature. The occupancies show a preference of  $\text{Fe}^{2+}$  to occupy the larger, M2 site ( $\sim 90\%$   $\text{Fe}^{2+}$ ), with M1 exhibiting a much lower iron percentage ( $\sim 65\%$ ). However, the ordering is not as pronounced as in the sample S95 of Nestola et al. (2008), where the  $\text{Fe}^{2+}$  SOFs were 82% and 8%, respectively. The refined Fe/Mg occupancy model for  $\text{Fs}_{82}$  is in good agreement with EMPA results. The value of the intracrystalline distribution coefficient  $-\ln k_D^*$ , calculated from the refined SOFs for the  $\alpha$ -opx

Table 1

Unit cell parameters of  $\text{Fs}_{82}$  determined from single crystal X-ray diffraction data at different pressures.

$p$ [GPa]	exp #	$a$ [Å]	$b$ [Å]	$c$ [Å]	$\beta$ [deg.]	$V$ [Å <sup>3</sup> ]
1.00E-04	0	18.383(1)	9.012(1)	5.2344(6)	90	867.17(3)
1.5(1)	2	18.323(47)	8.967(2)	5.2121(12)	90	856.3(22)
2.5(1)	1	18.281(3)	8.931(1)	5.2035(22)	90	849.5(4)
4.8(1)	2	18.229(58)	8.859(2)	5.1744(13)	90	835.5(27)
5.9(1)	1	18.192(3)	8.818(1)	5.1666(21)	90	828.8(4)
8.3(1)	2	18.139(61)	8.760(2)	5.1369(13)	90	816.2(28)
9.5(1)	3	18.117(4)	8.729(2)	5.1228(7)	90	810.1(3)
10.1(1)	2	18.101(64)	8.706(2)	5.1201(13)	90	806.9(29)
11.1(1)	1	18.183(7)	8.759(3)	5.0088(50)	91.96(5)	797.3(9)
12.3(1)	3	18.156(8)	8.735(4)	4.9887(12)	92.27(2)	790.6(6)
13.0(1)	3	18.188(9)	8.776(5)	4.8688(13)	90	777.1(6)
14.6(1)	1	18.142(4)	8.728(1)	4.8537(26)	90	768.6(5)
18.4(1)	1	18.057(3)	8.665(2)	4.8079(18)	90	752.3(4)
21.5(1)	1	18.024(4)	8.622(2)	4.7882(25)	90	744.1(5)
23.3(1)	3	17.978(8)	8.610(5)	4.7700(9)	90	738.3(6)
25.5(1)	1	17.965(4)	8.572(2)	4.7518(21)	90	731.7(4)
29.0(1)	1	17.884(5)	8.514(3)	4.7345(28)	90	720.9(5)
32.3(1)	3	17.830(16)	8.487(10)	4.7069(13)	90	712.2(10)

phase is 1.578, which suggests temperature of formation of 1200 K (Stimpfl et al., 1999).

### 3. Results

The transformation of  $\text{Fs}_{82}$  from the ambient  $\alpha$ -opx to the monoclinic  $\beta$ -opx phase takes place between 10.1(1) and 11.1(1) GPa, which is lower than in the previously examined natural  $\text{OEn}_{87}$  (between 12.66 and 14.26 GPa, Zhang et al., 2012), indicating that the transition pressure is dependent on iron content. At 11.1(1) GPa, the unit cell parameters are  $a = 18.183(7)$  Å,  $b = 8.759(3)$  Å and  $c = 5.009(5)$  Å, and the  $\beta$  angle becomes  $91.96(5)^\circ$ , accompanied by a 1.2% volume discontinuity. As a result of the transformation, the crystal expands along the [100] and [001] directions by about 0.5%, while the [010] direction contracts by 2.2%, as shown in Fig. 1.

As a consequence of the symmetry lowering, the crystal undergoes pseudomerohedral twinning into two domains related by a mirror on (001). The changes in the single-crystal diffraction pattern are shown in Supplementary Fig. 2. The transformation is completely reversible (no signature of the twinning remains in the diffraction pattern after the reversal) and is characterized by negligible hysteresis. Because of this complete reversibility, we do not expect any microstructural evidence of the transformation to be quenched. Because of the twinning, our initial attempts at structure refinement starting from the model of the  $\beta$ -opx  $\text{En}_{87}$  (Zhang et al., 2012) were unsuccessful. Subsequent elimination of peaks corresponding simultaneously to both twin domains produced a peak intensity dataset which yielded a very satisfactory refinement ( $R1 = 5.7\%$  for all data). Since Zhang et al. (2012) did not experience similar difficulties in their structure refinement of  $\beta$ -opx  $\text{En}_{87}$ , we conclude that the extent of the problems with peaks simultaneously contributed by two twin domains depends on the orientation of the crystal in the diamond anvil cell. Similar to the case of  $\beta$ -opx  $\text{En}_{87}$ , the  $\beta$ -phase of  $\text{Fs}_{82}$ , while assuming monoclinic (clino-) symmetry, clearly preserves the topology of the opx structure.

Zhang et al. (2012) did not determine the (meta)stability range of  $\beta$ -opx  $\text{En}_{87}$ , however, other, non-diffraction based studies with  $\text{En}_{100}$ , e.g. Zhang et al. (2011), Lin (2003, 2004), Lin et al. (2005) indicate that there is no other discontinuity in the compressional behavior up to at least 25 GPa. Unlike  $\text{En}_{87}$ ,  $\beta$ - $\text{Fs}_{82}$  transforms to orthorhombic phase  $\gamma$  only 2–3 GPa above the first change, between 12.3(1) and 13.0(1) GPa. The unit cell parameters of the  $\gamma$ -opx phase at 13.0(1) GPa are  $a = 18.188(9)$  Å,  $b = 8.776(5)$  Å,  $c = 4.869(1)$  Å and the  $\beta$  angle returns to  $90^\circ$  again. The volume discontinuity accompanying the  $\beta$ - $\gamma$  transition is 1.7%, with changes in individual unit cell parameters very similar to the first transition ( $a$  expands by 0.2%,  $b$  expands by 0.5%,  $c$  contracts by 2.4%). The twinning introduced in the  $\beta$ -phase disappears as the crystal assumes orthorhombic symmetry again in  $\gamma$ -opx. Similar to the first transformation, the  $\beta$ - $\gamma$  transition is also reversible and involves only negligible hysteresis. Structure refinement using data collected at 14.6(1) GPa yielded a model consistent with the orthorhombic phase HP-OEn1 predicted by Jahn (2008) for  $\text{En}_{100}$  above 20 GPa.

The crystal structures of the three opx phases are compared in Figs. 2 and 3. In  $\text{Fs}_{100}$  at ambient condition, both tetrahedral chains have the O-configuration, however, the rotation towards the ideal O-arrangement is much more pronounced in the SiB chain, with the O3–O3–O3 tetrahedral kinking angle  $T_kB = 143.7(2)^\circ$ , whereas for the SiA chain  $T_kA = 169.1(3)^\circ$  (Sueno et al., 1976)<sup>2</sup> is much closer

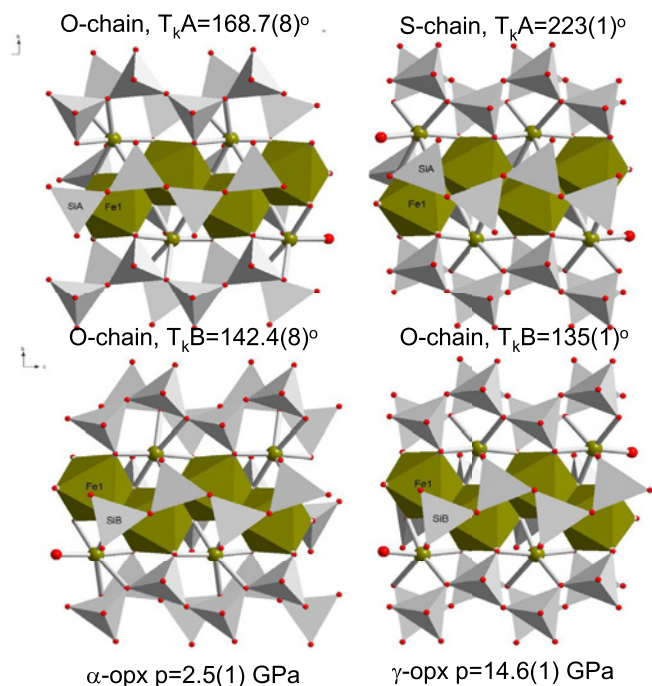


Fig. 2. Comparison of crystal structures and different configurations of tetrahedral chains in  $\alpha$ -opx at 2.5(1) GPa and  $\gamma$ -opx at 14.6(1) GPa, viewed along the [100] direction.

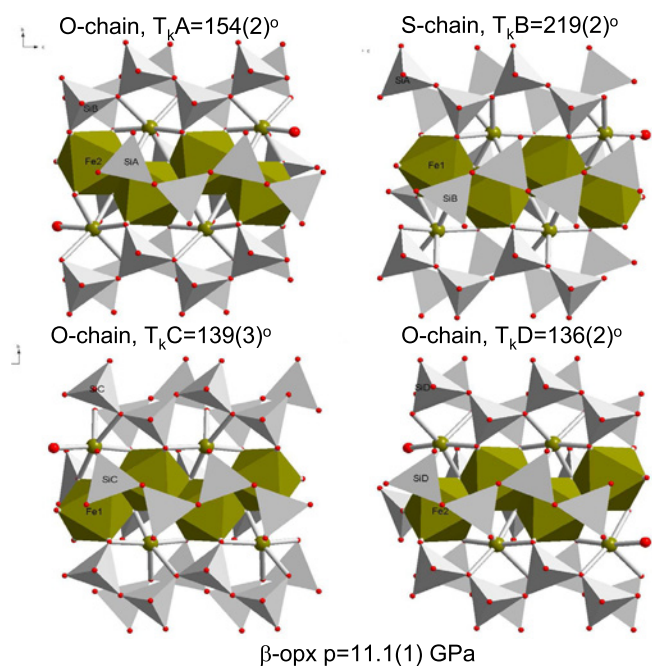


Fig. 3. Comparison of different configurations of tetrahedral chains in  $\beta$ -opx at 11.1(1) GPa viewed along the [100] direction.

<sup>2</sup> Some authors, including Sueno et al. (1976) use the O3A–O3A–O3A angle values greater than  $180^\circ$  for ease of comparison with cpx, despite that the SiA chain is O-rotated (ideal angle for the O-type chain is  $120^\circ$ ). Throughout this paper we use angles  $<180^\circ$  for the O-type chains and  $>180^\circ$  for the S-type chains.

to the extended configuration (for E-chains  $T_k = 180^\circ$ ). On compression the SiB chain rotates further towards the ideal O configuration ( $T_k$  decreases), while the trend for SiA chain is less well defined (Hugh-Jones et al., 1997; Nestola et al., 2008). The tetrahedral angles obtained from our refinement for  $\alpha$ -opx at 2.5(1) GPa are  $T_kA = 168.7(8)^\circ$  and  $T_kB = 142.4(8)^\circ$ , which is consistent with the general trends.

In the  $\alpha$ -opx phase at ambient pressure the polyhedral volumes of the M1 and M2 sites are 12.81 and 13.42 Å<sup>3</sup>, with the geometry of the M2 site much more distorted than M1, as indicated by the values of angle variance of 28.67, and 181.20, respectively (Sasaki et al., 1982). The octahedral geometry parameters obtained for Fs<sub>82</sub> at 2.5(1) GPa are 12.21 and 13.13 Å<sup>3</sup> for polyhedral volumes and 21.56 and 177.05 for angle variance, respectively. At ambient pressure, of the two SiO<sub>4</sub> tetrahedra, SiA has slightly smaller polyhedral volume (2.18 vs. 2.24 Å<sup>3</sup>) and is more distorted (angle variance for the two tetrahedral sites is 30.95 and 17.08, Sasaki et al., 1982). In Fs<sub>82</sub> at 2.5(1) GPa the tetrahedral volumes are 2.15 and 2.21 Å<sup>3</sup>, while angle variances are 32.27 and 16.78.

As expected, the main structural change involved in the  $\alpha$ - $\beta$  opx transition results from tetrahedral rotation. In the  $\beta$ -opx structure there are four symmetry independent Si chains (Fig. 3). Three of these, SiA, SiC and SiD are O-type, with  $T_kA = 154(2)^\circ$ ,  $T_kC = 139(2)^\circ$  and  $T_kD = 136(2)^\circ$ . The fourth chain, SiB, converts to S-type with  $T_kB = 219(2)^\circ$ . The SiA and SiB sites are located within the same tetrahedral layer, and the SiA O-chain sharing the layer with the SiB S-chain is the closest to the E configuration. The change in the average polyhedral volumes of the Si tetrahedra after the  $\alpha$ - $\beta$  transition is negligible ( $\Delta V_T = -0.2\%$ ), whereas both M1 and M2 sites compress by more than 4% with respect to  $\alpha$ -opx at 2.5(1) GPa. All of the coordination polyhedra, except for Si1 become more regular in the  $\beta$ -opx Fs<sub>82</sub>.

In  $\gamma$ -opx Fs<sub>82</sub>, the tetrahedral layers become uniform again (contain only one type of tetrahedral chain), with SiA becoming strongly S-type ( $T_kA = 223(1)^\circ$ ), while SiB remains strongly O-type ( $T_kB = 135(1)^\circ$ ) (Fig. 2). The changes in polyhedral geometry after the transformation to  $\gamma$ -opx are similar to the first transition, with tetrahedra contracting by 0.8%, and M1 and M2 sites contracting by 2.4% and 1.3%, respectively. The angular variance for SiA, SiB, and M1 polyhedra increases to values close to the  $\alpha$ -opx phase, whereas the M2 octahedron becomes even more regular than in  $\beta$ -opx, with the variance decreasing to 42.36 at 14.6(1) GPa.

### 3.1. Equation of state and molar volume relations

In light of the new phase transitions in Fs it is important to take a closer look at the density relations between all known polymorphs with Fs composition in the context of the thermodynamics of the opx-cpx transformation and pyroxene decomposition reactions. The bulk moduli for the different pyroxene phases for compositions close to the En-Fs join are summarized in Supplementary Table 1.

The bulk modulus does not change significantly with the Mg/Fe ratio, accompanying the En-Fs substitution and the values of the moduli obtained for our Fs<sub>82</sub> sample,  $K_0 = 113(2)$  GPa and  $K' = 6.1(2)$  are close to those for pure end members, and are consistent with the trend. EOS fit with  $K_0$  fixed to 101.0 GPa, the value obtained from Brillouin measurements on Fs<sub>100</sub> at ambient pressure (Bass and Weidner, 1984) gives  $K' = 9.8(4)$ .

The lp-hp clinopyroxene transition, because of its subtle displacive character is known to have a rather negligible effect on the elastic moduli, while changing  $V_0$  by about 2%. We find the  $\alpha$ - $\gamma$  transformation in opx, very similar in the structural mechanism to its lp-hp cpx counterpart, to also have similarly small effect on the elastic properties, with the  $\gamma$ -phase characterized by  $K_0 = 117(8)$  GPa,  $K' = 5.1(5)$ , remaining virtually unchanged (to within experimental uncertainty) and  $V_0 = 849(3)$  Å<sup>3</sup> reduced by 2% with respect to the  $\alpha$ -opx phase.

### 3.2. Elastic anisotropy

In the application of elasticity theory to geophysical modeling, an assumption is often made that the medium is elastically isotropic. However, most rock-forming minerals exhibit some degree of

elastic anisotropy, and any kind of preferred orientation of mineral grains within the rock will cause the rock to exhibit macroscopic elastic anisotropy as well (Thomsen, 1986). Orthopyroxenes are known to be elastically anisotropic. The sample S95 examined by Nestola et al. (2008) was shown to have axial compression anisotropy of  $\beta_a:\beta_b:\beta_c = 1.00:1.64:1.16$ , whereas Bass and Weidner (1984) obtained  $\beta_a:\beta_b:\beta_c = 1.00:1.46:1.13$  for Fs<sub>100</sub>. Results of fitting a quadratic equation to the pressure dependence of the unit cell parameters of our sample in the  $\alpha$ -opx phase give  $\beta_a = -0.0021(1)$  GPa<sup>-1</sup>,  $\beta_b = -0.0039(2)$  GPa<sup>-1</sup>,  $\beta_c = -0.0024(2)$  GPa<sup>-1</sup>, with  $\beta_a:\beta_b:\beta_c = 1.00:1.86:1.14$ . The main difference between these three results is the compressibility along the [010] direction (within the layer, perpendicular to Si-chains), most likely related to the compositional difference in Fe<sup>2+</sup> content and its ordering between the M1 and M2 sites. Because of the limited data for the  $\beta$ -opx (only two points) we could not reliably evaluate the anisotropy of compressibility of this phase. For the  $\gamma$ -opx phase the relations between the softest and stiffest directions remain the same with  $\beta_a = -0.0012(3)$  GPa<sup>-1</sup>,  $\beta_b = -0.0028(3)$  GPa<sup>-1</sup>,  $\beta_c = -0.0026(5)$  GPa<sup>-1</sup>, but the compressibility ratios change rather dramatically and become  $\beta_a:\beta_b:\beta_c = 1.00:2.33:2.17$ . The main factor accounting for this change is significant stiffening (by almost a factor of two) of the crystal along the [100] direction (normal to the layers). Ca-poor clinopyroxenes are known to stiffen as a result of the P2<sub>1</sub>/c-C2/c transition (e.g. Alvaro et al., 2011), but the direction of the largest change in compressibility in that case is [010], rather, than [100].

Because of the layered character and anisotropy of the pyroxene structure the factors controlling the three linear compressibilities of the crystal differ.  $C_{33}$  is the most variable of the longitudinal moduli as a function of opx composition, and is the most sensitive to structural variations, in particular to the configuration of the tetrahedral chains. Vaughan and Bass (1983) postulated that a threshold kinking angle may exist, below which the tetrahedral chain is passive and the octahedral layer becomes the dominating structural support element.  $C_{11}$  is the longitudinal modulus most constant as a function of opx composition. Bass and Weidner (1984) suggested that it is linearly related to the compressibility of the smaller and stiffer M1 octahedra. Surprisingly, our linear compressibility data indicate that despite the significant discontinuous changes in the tetrahedral kinking angle across the  $\alpha$ - $\beta$ - $\gamma$ -opx transitions, the compressibility along [001] changes the least, whereas the drastic change in stiffness along [100] happens despite a very small, 2.4% change in the average M1-O bond length from 2.5(1) to 14.6(1) GPa, suggesting that the interplay between different structural controls of elasticity is more complex than previously assumed.

## 4. Discussion and conclusion

Elastic properties of principal mantle minerals, including orthoferrosilite and volume/density relations between their polymorphs, are fundamental parameters in geophysical modeling of the composition, properties and seismic structure of the Earth (Stixrude and Lithgow-Bertelloni, 2005; Xu et al., 2008) and extra-terrestrial bodies (e.g. Verhoeven et al., 2005). Consequently, information about significant discontinuities and new polymorphic transitions of the mantle minerals should be included in these models. The two new displacive structural transitions in Fs<sub>82</sub> demonstrate that after completion of the  $\beta$ - $\gamma$  opx transformation, at pressures above 12.3(1) GPa the density of orthopyroxene becomes comparable to that of the high-pressure clinopyroxene. While opx is still most likely to remain metastable at higher pressures, the two opx transitions are very likely to cause discontinuities in the opx-cpx phase boundary. In the low pressure range, the P2<sub>1</sub>/c-C2/c phase transition in cpx has a very dramatic effect on the opx-cpx Clapeyron slope and because of the similarity be-

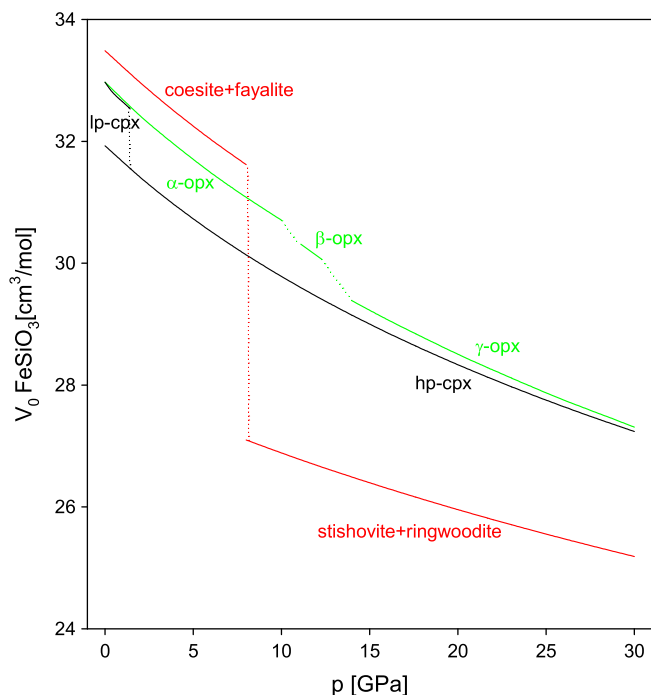


**Fig. 4.** Pressure evolution of the molar volume of  $\text{FeSiO}_3$  in different phases of opx and cpx compared with the equivalent molar volume of pyroxene decomposition products.

tween the  $\alpha$ - $\beta$ - $\gamma$  opx and lp-hp cpx transitions, we expect that the opx-cpx Clapeyron slope will show two corresponding discontinuities above 10 GPa.

The estimated entropy changes  $\Delta S$  for both opx-cpx and lp-hp cpx transitions are negative, which means that enthalpy, and the associated volume change work are the factors driving the transitions (Angel and Hugh-Jones, 1994). Both transitions are endothermic and have positive latent heat. In order for the Gibbs free energy of the higher-pressure polymorphs to decrease, the  $P\Delta V$  term needs to compensate for both the entropic change and the latent heat. Similarly, for the decomposition reaction of  $\text{Fe}_2\text{Si}_2\text{O}_6$  to  $\text{SiO}_2$  and  $\text{Fe}_2\text{SiO}_4$ , the entropic effect of the volume change, which dramatically increases with the coesite-stishovite transformation, determines the reaction boundary in the  $P$ - $T$  space. In Fig. 4 we compare the molar volumes<sup>3</sup> of  $\text{FeSiO}_3$  in  $\alpha$ -opx,  $\beta$ -opx,  $\gamma$ -opx, lp-cpx, hp-cpx,  $\text{SiO}_2$ (coesite)+ $\alpha$ - $\text{Fe}_2\text{SiO}_4$  and  $\text{SiO}_2$ (stishovite)+ $\gamma$ - $\text{Fe}_2\text{SiO}_4$ . Since our sample had an intermediate solid solution composition, we applied a 1% volume correction, which makes  $V_0$  of  $\text{Fs}_{82}$  equal to  $\text{Fs}_{100}$ . As discussed above, the possible effect of the Mg content on the bulk modulus in  $\text{Fs}_{82}$  is most likely not significant. As can be seen in Fig. 4, the molar volumes of  $\alpha$ -opx and lp-cpx are approximately equal at ambient temperature, over the whole stability range of lp-cpx, which means that the volume work advantage of the opx-cpx conversion is negligible. As long as coesite, or lower pressure tetrahedral  $\text{SiO}_2$  phases are the products of the decomposition reaction, the volume change accompanying this reaction is positive (reaction is thermodynamically unfavorable). The lp-hp cpx transition lowers the molar volume of cpx by about 2%, which makes the  $P\Delta V$  term for opx-cpx conversion significant, and further stabilizes the pyroxene with respect to the decomposition. Above approximately 8 GPa the stishovite phase of  $\text{SiO}_2$  becomes stable, and  $\text{Fe}_2\text{SiO}_4$  transforms to

the  $\gamma$ -phase, changing the molar volume of the decomposition products by more than 30% and strongly favoring that reaction. The  $\alpha$ - $\beta$  transition in opx above 10.1(1) GPa reduces the volume change for opx-cpx conversion by about half, and the further transformation to  $\gamma$ -opx above 12.3(1) GPa makes the volumes of opx and cpx almost equal (at 30 GPa the cpx density remains higher by about 1%). We expect that both of the opx transitions would have a discontinuous effect on the opx-cpx conversion, shifting the phase boundary to higher pressures and extending the opx stability field, however, cpx is likely to remain the most stable of pyroxene phases above 10 GPa. The increase in density in the  $\gamma$ -opx phase is not sufficient to fully compensate the  $P\Delta V$  effect of the decomposition reaction above the coesite-stishovite phase boundary, and the decomposition is still going to be favored at higher pressures. Because of the molar volume relations shown in Fig. 4, it seems most likely that the metastability of  $\beta$ - and  $\gamma$ -opx phases with respect to the hp-cpx structure is kinetic in nature, caused by a high activation barrier  $\Delta G^{\ddagger}$  of the opx-cpx conversion, rather than by a reversal of the sign of  $\Delta G$ .

In Fe-poor opx compositions, the pressure of the more significant  $\beta$ - $\gamma$  transition is shifted to much higher pressures (likely to above 25 GPa for pure  $\text{En}_{100}$ , Lin, 2003, 2004; Lin et al., 2005), making the iron content of natural pyroxenes a critical parameter affecting the phase equilibria.

Information about the new phase transitions in opx provides an improved understanding of the crystal chemical trends and transformation paths of opx to higher-pressure minerals with 6-coordinated Si. The mechanisms of the  $\alpha$ - $\beta$  and  $\beta$ - $\gamma$  transitions, involving purely tetrahedral rotation are fully consistent with trends known for the pyroxene family, but demonstrate new possibilities for discontinuous re-arrangements of the opx structure (Downs, 2003). Recently, Plonka et al. (2012) described a new high-pressure phase of diopside, constituting an intermediate step of cpx breakdown to  $\text{MgSiO}_3$  akimotoite and  $\text{CaSiO}_3$  perovskite, with Si assuming octahedral coordination. The two new phase transitions in  $\text{Fs}_{82}$  are a likely prelude to similar metastable conversion in orthopyroxenes.

Quenchable microstructural features resulting from polymorphic transitions at high pressures and temperatures are often used as proxies for the thermodynamic history of natural samples (Bozhilov et al., 1999; Schmitz and Brenker, 2008), however, both of the new transformations in  $\text{Fs}_{82}$  are fully reversible and not expected to leave microstructural signatures usable as thermobarometry clues.

Our results indicate a significant change of the elastic anisotropy of opx across the polymorphic phase transitions. This change could have seismically detectable consequences for the subducted slabs, perhaps more significant than the subtle discontinuities in the density and bulk modulus. High-pressure rocks in collisional orogens such as Alpine eclogites, regarded as relics of subduction zones, have been demonstrated to contain pyroxenes (particularly omphacite) characterized by a significant degree of lattice preferred orientation (Bascou et al., 2001; Bascou et al., 2002), which further supports the notion of possible seismic detectability of the transformations reported here.

#### Acknowledgements

This work was performed at HPCAT (Sector 16) and GeoSoilEnviroCARS (Sector 13), Advanced Photon Source (APS), Argonne National Laboratory. HPCAT operations are supported by CIW, CDAC, UNLV and LANL through funding from DOE-NNSA and DOE-BES, with partial instrumentation funding by NSF. GeoSoilEnviroCARS is supported by the National Science Foundation - Earth Sciences (EAR-1128799) and Department of Energy - Geosciences (DE-FG02-94ER14466). Use of the Advanced Photon Source was supported by the U. S. Department of Energy,

<sup>3</sup> Equation of state data used to calculate the molar volumes were taken from Speziale et al. (2004) for fayalite, Nestola et al. (2010) for Fe-ringwoodite, Angel et al. (2001) for coesite, Nishihara et al. (2005) for stishovite, Hugh-Jones et al. (1994) for lp-CFs and Xu et al. (2008) for hp-CFs.

Office of Science, Office of Basic Energy Sciences, under Contract No. DE-AC02-06CH11357.

## Appendix A. Supplementary data

Supplementary data associated with this article can be found, in the online version, at <http://dx.doi.org/10.1016/j.pepi.2013.06.006>.

## References

- Akashi, A., Nishihara, Y., et al., 2009. Orthoenstatite/clinoenstatite phase transformation in MgSiO<sub>3</sub> at high-pressure and high-temperature determined by in situ X-ray diffraction: Implications for nature of the X discontinuity. *J. Geophys. Res.* 114, B04206.
- Akimoto, S.-i., Syono, Y., 1970. High-pressure decomposition of the FeSiO<sub>3</sub>–MgSiO<sub>3</sub>. *Phys. Earth Planet. Inter.* 3, 186–188.
- Alvaro, M., Nestola, F., et al., 2011. High-pressure displacive phase transition of a natural Mg-rich pigeonite. *Phys. Chem. Miner.* 38, 379–385.
- Angel, R.J., 2000. Equations of state. *Rev. Mineral. Geochem.* 41, 35–59.
- Angel, R.J., Hugh-Jones, D.A., 1994. Equations of state and thermodynamic properties of enstatite pyroxenes. *J. Geophys. Res.* 99, 19777–19783.
- Angel, R.J., Mosenfelder, J.L., et al., 2001. Anomalous compression and equation of state of coesite. *Phys. Earth Planet. Inter.* 124, 71–79.
- Bascou, J., Barruol, G., et al., 2001. EBSD-measured lattice-preferred orientations and seismic properties of eclogites. *Tectonophysics* 342, 61–80.
- Bascou, J., Tommassi, A., et al., 2002. Plastic deformation and development of clinopyroxene lattice preferred orientations in eclogites. *J. Struct. Geol.* 24, 1357–1368.
- Bass, J.D., Weidner, D.J., 1984. Elasticity of single-crystal orthoferrosilite. *J. Geophys. Res.* 89, 4359–4373.
- Bina, C.R., Stein, S., et al., 2001. Implications of slab mineralogy for subduction dynamics. *Phys. Earth Planet. Inter.* 127, 51–66.
- Bown, M.G., 1965. Re-investigation of clino-ferrosilite from Lake Naivasha, Kenya. *Mineral. Mag.* 34, 66–70.
- Bozhilov, K.N., Green, H.W., et al., 1999. Clinoenstatite in alpe arami peridotite: additional evidence of very high pressure. *Science* 284 (128–132).
- Brothers, R.N., Yokoyama, K., 1990. Fe-rich pyroxenes from a microdiorite dike, Whangarei, New Zealand. *Am. Mineral.* 75, 620–630.
- Dera, P., Lazarz, J.D., et al., 2011. Pressure-induced development of bonding in NiAs type compounds and polymorphism of NiP. *J. Solid State Chem.* 184, 1997–2003.
- Dera, P., Zhuravlev, K., Prakapenka, V., Rivers, M.L., Finkelstein, G.J., Grubor-Urošević, O., Tschauer, O., Clark, S.M., Downs, R.T., 2013. High-pressure single-crystal micro-X-ray diffraction (SCmXRD) analysis with GSE, ADA/RSV software. *High Pressure Res.* <http://dx.doi.org/10.1080/08957959.2013.806504>.
- Dove, M.T., Heine, V., et al., 1995. Rigid unit modes in framework silicates. *Mineral. Mag.* 59, 629–639.
- Downs, R.T., 2003. Topology of the pyroxenes as a function of temperature, pressure, and composition as determined from the procrystal electron density. *Am. Mineral.* 88, 556–566.
- Frost, D.J., 2008. The upper mantle and transition zone. *Elements* 4, 171–176.
- Hugh-Jones, D., Woodland, A.B., et al., 1994. The structure of high-pressure C2/c ferrosilite and crystal chemistry of high-pressure C2/c pyroxenes. *Am. Mineral.* 79, 1032–1041.
- Hugh-Jones, D., Sharp, T., et al., 1996. The transition of orthoferrosilite to high-pressure C2/c clinoferrosilite at ambient temperature. *Eur. J. Mineral.* 8, 1337–1345.
- Hugh-Jones, D., Chopelas, A., et al., 1997. Tetrahedral compression in (Mg, Fe)SiO<sub>3</sub> orthopyroxenes. *Phys. Chem. Miner.* 24, 301–310.
- Jackson, J.M., Sinogeikin, S.V., Carpenter, M.A., Bass, J.D., 2004. Novel phase transition in orthoenstatite. *Am. Mineral.* 89, 239–245.
- Jaffe, H.W., Robinson, P., et al., 1978. Orthoferrosilite and other iron-rich pyroxenes in micropelite gneiss of the Mount Marcy area, Adirondack Mountains. *Am. Mineral.* 63, 1116–1136.
- Jahn, S., 2008. High-pressure phase transitions in MgSiO<sub>3</sub> orthoenstatite studied by atomistic computer simulation. *Am. Mineral.* 93, 528–532.
- Lin, C.-C., 2003. Pressure-induced metastable phase transition in orthoenstatite (MgSiO<sub>3</sub>) at room temperature: a Raman spectroscopic study. *J. Solid State Chem.* 174, 403–411.
- Lin, C.-C., 2004. Pressure-induced polymorphism in enstatite (MgSiO<sub>3</sub>) at room temperature: clinoenstatite and orthoenstatite. *J. Phys. Chem. Solids* 65, 913–921.
- Lin, C.-C., Chao, J.-L., et al., 2005. Metastable phase transition of orthoenstatite (MgSiO<sub>3</sub>) under high pressure. *Solid State Sci.* 7, 293–297.
- Lindsley, D.H., 1983. Pyroxene thermometry. *Am. Mineral.* 68, 477–493.
- Lindsley, D.H., Davis, B., et al., 1964. Ferrosilite (FeSiO<sub>3</sub>); synthesis at high pressure and high temperature. *Science* 144, 73.
- Liu, L.-G., 1976. The high-pressure phases of FeSiO<sub>3</sub> with implications for Fe<sub>2</sub>SiO<sub>4</sub> and FeO. *Earth Planet. Sci. Lett.* 33, 101–106.
- Mao, H.K., Xu, J., et al., 1986. Calibration of the ruby pressure gauge to 800 kbar under quasi-hydrostatic conditions. *J. Geophys. Res.* 91, 4673–4676.
- Ming, L.-C., Bassett, W.A., 1975. High-pressure phase transformations in the system MgSiO<sub>3</sub>–FeSiO<sub>3</sub>. *Earth Planet. Sci. Lett.* 27, 85–89.
- Nestola, F., Boffa-Ballaran, T., et al., 2008. The high-pressure behavior of an Al- and Fe-rich natural orthopyroxene. *Am. Mineral.* 93, 644–652.
- Nestola, F., Ballaran, T.B., et al., 2010. New accurate compression data for g-Fe<sub>2</sub>SiO<sub>4</sub>. *Phys. Earth Planet. Inter.* 183, 421–425.
- Nishi, M., Kato, T., et al., 2008. Survival of pyropic garnet in subducting plates. *Phys. Earth Planet. Inter.* 170, 274–280.
- Nishihara, Y., Nakayama, K., et al., 2005. P-V-T equation of state of stishovite to the mantle transition zone conditions. *Phys. Chem. Miner.* 31, 660–670.
- Plonka, A., Dera, P., et al., 2012. B-diopside, a new ultrahigh-pressure polymorph of CaMgSi<sub>2</sub>O<sub>6</sub> with six-coordinated silicon. *Geophys. Res. Lett.* 39, L24307.
- Polí, S., Schmidt, M.W., 2002. Petrology of the subducted slabs. *Annu. Rev. Earth Planet. Sci.* 30, 207–235.
- Ramberg, H., DeVore, G.W., 1951. The distribution of Fe<sup>2+</sup> and Mg<sup>2+</sup> in co-existing olivines and pyroxenes. *J. Geol.* 59, 193–210.
- Rivers, M.L., Prakapenka, V.B., et al., 2008. The COMPRES/GSECARS gas loading system for diamond anvil cells at the Advanced Photon Source. *High Pressure Res.* 28, 273–292.
- Sasaki, S., Takeuchi, Y., et al., 1982. Electron-density distributions of three orthopyroxenes, Mg<sub>2</sub>Si<sub>2</sub>O<sub>6</sub>, Co<sub>2</sub>Si<sub>2</sub>O<sub>6</sub>, and Fe<sub>2</sub>Si<sub>2</sub>O<sub>6</sub>. *Z. Kristallogr.* 158, 279–297.
- Saxena, S.K., Ghose, S., 1971. Mg<sup>2+</sup>–Fe<sup>2+</sup> order-disorder and the thermodynamics of the orthopyroxene crystalline solution. *Am. Mineral.* 56, 532–559.
- Schmitz, S., Brenker, F.E., 2008. Microstructural indications for protoenstatite precursor of cometary MgSiO<sub>3</sub> pyroxene: a further high-temperature component of comet Wild 2. *Astrophys. J.* 681, L105–L108.
- Schreyer, W., Stepto, D., et al., 1978. Clinoelute (magnesian clinoferrosilite) in a eulysite of a metamorphosed iron formation in the vredefort structure, South Africa. *Contrib. Mineral. Petrol.* 65, 351–361.
- Sheldrick, G.M., 2008. A short history of SHELX. *Acta Crystallogr.* A64, 112–122.
- Speziale, S., Duffy, T.S., et al., 2004. Single-crystal elasticity of fayalite to 12 GPa. *J. Geophys. Res.* 109, B12202.
- Stimpfl, M., Ganguly, J., et al., 1999. Fe<sup>2+</sup>–Mg order-disorder in orthopyroxene: equilibrium fractionation between the octahedral sites and thermodynamic analysis. *Contrib. Mineral. Petrol.* 136, 297–309.
- Stixrude, L., Lithgow-Bertelloni, C., 2005. Thermodynamics of mantle minerals – I. Physical properties. *Geophys. J. Int.* 162, 610–632.
- Sueno, S., Cameron, M., et al., 1976. Orthoferrosilite: high-temperature crystal chemistry. *Am. Mineral.* 61, 38–53.
- Thompson, R.M., Downs, R.T., 2003. Model pyroxenes I: ideal pyroxene topologies. *Am. Mineral.* 88, 653–666.
- Thomsen, L., 1986. Weak elastic anisotropy. *Geophys.* 51, 1954–1966.
- Vaughan, M.T., Bass, J.D., 1983. Single-crystal properties of protoenstatite: a comparison with orthoenstatite. *Phys. Chem. Miner.* 10, 62–68.
- Verhoeven, O., Rivoldini, A., et al., 2005. Interior structure of terrestrial planets: modeling Mars' mantle and its electromagnetic, geodetic, and seismic properties. *J. Geophys. Res.* 110, E04009.
- Weber, H.P., 1983. Ferrosilite III, the high-temperature polymorph of FeSiO<sub>3</sub>. *Acta Crystallogr.* C39, 1–3.
- Xu, W., Lithgow-Bertelloni, C., et al., 2008. The effect of bulk composition and temperature on mantle seismic structure. *Earth Planet. Sci. Lett.* 275, 70–79.
- Young, D.A., Cuthbertson, J., 1994. A new ferrosilite and Fe-pigeonite occurrence in the reading prong, New Jersey, USA. *Lithos* 31, 163–176.
- Zhang, D., Jackson, J.M., et al., 2011. Local structure variations observed in orthoenstatite at high pressures. *Am. Mineral.* 96, 1585–1592.
- Zhang, J., Dera, P., et al., 2012. A new high-pressure phase transition in iron-bearing orthoenstatite: an anisotropy discontinuity in the upper mantle? *Am. Mineral.* 97, 1070–1074.